Annual cycle of the land surface temperatures over East Asia in connection with agricultural activities

Gyu-Ho Lim
SEES, Seoul National University, Gwanak-Ro 1, Gwanak-Gu, Seoul, South Korea
gyuholim@snu.ac.kr

Abstract

By applying Harmonic Analysis of Time Series (HANTS) to the time series of the pixel-wise land surface temperature (LST) from the Tera and Aqua satellite observations, we decomposed the climatological annual cycle of the LST into the various frequency components and examined their horizontal distribution over East Asia. The frequency component 1 $year^{-1}$ expressed the regular seasonal change in a year. The component 2 $year^{-1}$ revealed the meridional displacement of the east-west oriented rain belt, and the frequency 3 $year^{-1}$ represented the temperature change due to agricultural activity over the double crop region of the North China Plain (NCP). In addition to the high-temperature condition nearly coinciding with the time of the first crop harvest, there existed another warm period in the autumn season that appeared in the most of the analysis domain.

1. Introduction

The ecological landscape forms from the bilateral interaction of the physical conditions and biological processes rather than a one-way process between them. Men's agricultural activities changed the ecological state of the surface of the earth. As farming techniques improve, it is common to practice monoculture on a large scale for economic feasibility. The modern state of farming has a great impact on the land surface characteristics, which may not be negligible for understanding the earth's climate.

Many authors tried to understand the relationship between the landuse and the climate change (Bonan 2001; Cooley et al. 2005; Nair et al. 2007; Lee et al. 2009; Ge 2010; Yamashima et al. 2011; Ho et al. 2012). With continual increase of the greenhouse gasses and aerosol loading in the atmosphere, the Earth surface change resulted from farming becomes one of the non-negligible man-made effects on the climate change. As cultivation area expands and agricultural productivity increases, the climatic effect of the farm land coverage needs to be considered as well as the other elements leading to climate change such as increasing atmospheric carbon dioxide and the sea surface temperatures (Ho et al. 2012).

Among the various types of landuse, the areal expansion of cultivation might have influenced the regional climate and the associated atmospheric circulation (Takata, Saito, and Yasunari 2009; Yamashima et al. 2011). Temporal variation of land surface conditions from farming modified the near-surface fluxes of heat and water vapor (Osborne et al. 2009). Ge (2010) showed a similar change by farming, especially after harvest, of the southern Great Plains of North America. Many authors pointed out that the crop harvest significantly modified the fluxes of energy, momentum, and water vapor from the land surface to the overlying atmosphere (Cooley et al. 2005; Pielke et al. 2007). The climate response to the type of landuse may reach to the regional and global scales rather than confined to the local area only (Ray et al.

2006; Nair et al. 2007; Pielke et al. 2007).

Ho et al. (2012) emphasized the possible effects of the multi-crop activities, which could induce the warmer and drier conditions from their analysis of the NCP where the double crop was common. They also suggested that such multi-crop behavior would cause a severe water balance problem in the region. For their comprehensive analysis of the region, they employed diverse data sets such as LST, Normalized Difference Vegetation Index (NDVI), meteorological station temperatures.

Cho et al. (2014) investigated the possible impacts of the NCP agricultural activities on the regional climate. For diverse climate change scenarios, they analyzed the present and the future atmosphere circulations simulated with the ecological climate model by Cooley et al. (2005). Their analysis results showed that the land surface was warmer and drier after harvest, and the simulation was consistent with observations (Ho et al. 2012). The bare soil surface after harvest in June had biophysical impacts on the surface climate. The bare soil decreased evapotranspiration and latent heat flux from the surface.

To assess the effects of the type of farming on the land surface temperatures, we examined the annual progressing of land surface temperature by carrying out the Fourier frequency analysis of the time series of the LSTs at each pixel. With the aid of GRASS Development Team (2016), it is straightforward to extract a frequency component and associated quantities from the annual variation map time series composed of the 46 maps of the 8-day LSTs.

We like to assess any probable change in the annual march of the surface temperature in connection with the agricultural practice. For the purposes, we carefully compared the contributions to the total temperature values by each frequency component. This paper has following structure. Section 2 describes the data employed and analysis methods. Section 3 discussed the analysis results. We have drawn conclusions in Section 4.

2. Data and analysis methods

2.1. Data

We have downloaded the LST 8-day composites in digital numbers (DN) in an unsigned 16 bits integer format. The LST data were produced from the observations by the Moderate Resolution Imaging Spectroradiometer (MODIS). The pixel size of the downloaded image is 1 km. We reduced the pixel size approximately by half and obtained 520 meters resolution images. The resolution increment did not produce any side effects because of aggregation of many samples. We did not use the scale factor 0.02 for the conversion of DN to temperature scales in Kelvin or Celsius for reducing processing time.

The MODIS data have been well calibrated and examined for the study of crop related climate change, epidemiology, and other various research purposes (Wan et al. 2004; Wan and Li 2008; Bosilovich 2006; Ho et al. 2012; Zorer, 2013). With confidence in the accuracy of the satellite LST observations and a new processing technique, Metz et al. (2014) produced no gap temperature fields with a horizontal resolution of 250 meters and at the temporal interval of four times a day for the entire Europe. Version-5 MODIS/Terra LST/E product has been validated to a level, at which its accuracy is reliable over widely

distributed locations and extensive time periods. Further details regarding MODIS land product validation for the LST/E products are at the following website http://landval.gsfc.nasa.gov/ProductStatus.php?ProductID

By considering the previously mentioned accuracy and our unique object of analysis, we did not try further calibration or comparison with the corresponding weather station temperature values or other relevant parameters. In the analysis, we concentrated on the space and time variation of LST instead of its absolute value. The weather stations are in general in the lowland place and close to people's habitats. The placement may not be suitable to characterize the cropland and forest area temperatures.

As a preprocessing, we computed the mean climate values of the 8-day LSTs at a given time of the year. For the climate mean, we took an arithmetic averages of the minimum and maximum values from Tera and Aqua satellites, altogether, for the entire 11 years data period. While computing the mean values, we excluded gapped pixels at a given location and time. The ratio of missing events for each pixel is less than 3 % on average. We have 46 maps for a complete annual cycle. Time interval for each record covers eight days, but the last record extends for five days for a normal year and six days for a leap year.

In addition to the LST data, we have downloaded geographic information system (GIS) data such as digital elevation map and the coastline data from the website https://www.ngdc.noaa.gov/mgg/dem/ and used them wherever we need them for calculation and displaying. The backbone for the data processing was the geographical resources analysis supporting system (GRASS) by the GRASS Development Team (2016).

2.2. Analysis methods

In the satellite data processing arena, many authors used frequency analysis to estimate missing values and identify outliers (Menenti et al. 1993; Verhoef, Menenti, and Azzali 1996; Roerink, Menenti, and Verhoef 2000). For harmonic analysis, we used a package HANTS that is an external addition to the GRASS GIS. Detailed usage of the package is in Roerink et al. (2000), and some modification is in the add-on explanation of the GRASS manual.

By repeatedly applying the package to the annual LSTs with a different frequency option, we obtained the 46 maps-composing annual cycles for every category of combination of frequencies. Differing from the recommendation in the package manual, we computed for the number of frequencies option 1, 2, and 3. By the subsequent additions and subtractions, we obtained the map times series for a certain frequency or for a frequency band that is the combination of frequencies. For example, the map time series retaining the frequencies larger than and equal to 4 $year^{-1}$ were obtained by subtracting the map time series having frequency components 1-3 $year^{-1}$ from the observed LSTs, of which map time series contain all the frequency components.

We examined the internal consistency among the amplitudes and phases of the obtained frequency components. By computing the residuals or deviations of the observed annual map time series on the estimated annual cycles based on a given frequency or the frequency bands, we also checked the

contribution to the observed map time series at a particular time of the year. To keep the limited number of frequency components was conservative when considering the Nyquist frequency was 23 year^{-1}, where 23 Fourier frequencies were resolvable. After diverse testing of the number of frequencies to be retained, we concluded that the four categories of frequency components were reasonable for the analysis objects.

When applying HANTS for harmonic analysis, we did not use the range option. The fitness of error tolerance was 50 DN or 1 K. The selected criterion forced that the kept temperature values for the frequency curve fitting did not deviate from the fitted value by 1 K or more. The procedure of fitting excluded the observed values when their residual or deviation was larger than the threshold value for calculation.

3. Analysis results

3.1. Climatic LST distribution

In Figure 1(*a*), the primary spatial distribution of LST is inversely proportional to the latitudes. The next control element looks like to be the altitude of the position concerned. The others may be related with a further complication with the factors hard to explain. The topography is in the orange colored contours of which interval is 500 meters from the zero line that coincides with the coastline in Figure 1(*a*). From the near coincidence of the contours with LST color shading in the figure, the temperature dependency on the topography are discernable with ease.

Figure. 1(*b*) shows the distribution of the amplitudes of the frequency 3 year^{-1} (the third harmonic component) of the annual LST at each pixel. The red and blue rectangles mark the area for investigating 8-day LST change in the time domain for the annual cycle. For comparison, we included the amplitude and phase of the frequencies 1 year^{-1} and 2 year^{-1} as a supplement (S1). The amplitude of the both components was large over the high latitudes and high altitude places in general. And phase was almost the same over the entire analysis domain. In contrast with the horizontal pattern of the frequency components 1 year^{-1} and 2 year^{-1}, the frequency 3 year^{-1} showed large amplitudes over the NCP region mostly. The phase of frequency 3 year^{-1} was same only for a localized areal extent and much more complex than those of the frequencies 1 year^{-1} and 2 year^{-1} shown in the supplement.

3.2. Annual change in the 8-day LST

In Figure 2, the most notable feature is the regular LST change predicted by the frequency component 1 year^{-1}. The highest value of LST appeared near the 12th of July in the both regions of NCP and SWK. The maximum observed temperature reached around the 12th of July in NCP and 6th of June in SWK. Over the NCP, consequently, the annual maximum of the actual LST appeared before the predicted peak by the frequency component 1 year^{-1}. The former followed the latter in SWK. Over the DC region of NCP, the largest deviation of the observed LST from the frequency component 3 year^{-1} prediction appeared on June 18-25 or DOY 169-176 in a year.

The deviations of the observed annual cycle from each corresponding frequency component were much smaller in the single crop region (SWK) than in the NCP, as evident from Figure 2. For the single crop area, the annual temperature progression was well represented by the frequency 1 year^{-1} that resulted from the harmonic analysis. The temperature deviation from the functional value of the frequency 1 year^{-1} was less than about 2 K or 100 DN in Figure 2(*d*). The double crop region had a large contribution from the frequency 3 year^{-1} in Figure 2(*a*) and 2(*c*). In Figure 2(*b*), on the other hand, the frequency 3 year^{-1} contribution was nearly absent when considering the similar shape of dashed and dotted curves in magnitude and temporal changes in Figure 2(*d*).

The reversed solid triangle marks the time of the largest residual of the LST on the predictions by the various frequencies in Figure 2. The local maxima of residual appeared at the same time of the year in the both regions, which is apparent from comparison of Figures 2(*c*) and 2(*d*). The negative residuals for the frequency component 2 year^{-1} formed the summer time local minima in the both regions with a time difference of about half month in Figures 2(*c*) and 2(*d*). The time of occurrence and the time delay of the negative peaks between in the two regions suggests that the frequency 2 year mostly reflected the rainy season of East Asia. The rain band associated the wet season of East Asia migrated from south to north over the region for the period from the end part of June to the middle part of July in a year.

The single crop region had a significant contribution to the observed LST mostly from the frequency component 2 year^{-1} and a small portion from the other frequency components. The annual change manifested by frequency 2 year^{-1} might have a strong connection with the rainy season over the region. The summertime rainy season are well known in East Asia. It is called Jiangma in Korea, Meiu in China, and Baiu in Japan. With some variation in intensity, the phenomenon was regular and active over East Asia. The rainy season begin on average in the southern part of the Korean Peninsula on June 20 and lasted until July 10th or 20th (Lim et al. 1992, Jung et al. 2001). The rainy season certainly caused the mid-year coolness in the residual values in Figures 2(*c*) and 2(*d*).

We calculated and displayed the LST distribution for the two epochs of the year as marked with the solid and the empty reversed triangles in Figure 2. Figure 3 shows the contributed amount to the total LST by each frequency component or their combinations for the period of year: DOY 169-176 or June 18-25. From the maps in the figure, each frequency component contribution to the total LST was variable from place to place. The largest deviation appeared over the DC region in Figure 3(*d*). But the deviation was enlarged by the other frequency components. The amplification is notable from the overall increase of deviation in magnitude over the other regions. Therefore, the temperature change based on June minus May temperatures would inadvertently overestimate the surface temperature change solely resulting from the crop harvest. The specific reason is that high frequencies larger than 3 year^{-1} contributed to the temporal increase in temperature over the entire analysis domain.

Figure 4 shows the maps for the second warm period. The LST residuals on the frequency 1 year^{-1} (Full-H1) was positive in the northern part of the analysis domain and lower values in the south. Specifically, they were large over the Manchuria and the adjacent regions that were part of North Korea and Russia. We can observe a similar pattern in Figures 4(*c*) and 4(*e*) with reduced strength. At the same time, the inland water bodies had relatively small residual values than the neighboring land. For an example, we

can point out Lake Khanka straddling the borderline between China and Russia. The contrast merely implied that the sizable water body followed the temperature change controlled by the lower frequency components in general. The cooling rate of the water body was smaller compared with that of the surrounding land.

In the second warm epoch of the year, in other words autumn season of the regoins, the temporal change of the LST was the same for all the frequency components, but with some variation in magnitude.

4. Conclusions

The harmonic analysis can be used to reduce data volume for the analysis of annual cycle as well as for detecting and interpolating the cloud affected pixels in satellite observations of the surface temperature and vegetation as noted by Roerink et al. (2000). In our analysis, the three frequencies from the harmonic analysis exclusive of the frequency zero or time mean component, explained the most of the total variation associated with the annual progression of LST over East Asia, irrespective of the types of land cover and usage.

As consistent with many authors' findings, the DC region showed the rapid increase in temperature from the middle of May to the last part of June; the third frequency function could correctly model the rising temperature from cropping. A cool condition of May seemed to be well represented by the frequency 2 $year^{-1}$. Therefore, the second and third harmonics convincingly portrayed the temperature change possibly accompanied by the DC exercises and seasonal change of temperature in the NCP. In the southwest of the Korea Peninsula that was traditionally single crop region, the third harmonics contribution was minor as inferred from almost the same magnitude and temporal change of the dashed and the dotted curves of Figure 2(*d*).

Over the double crop region, the rapid increment in temperature for the time span of about one month from May 16-23 to June 18-25 reached about 7.5 K or 375 DNs, which were possible to estimate from Figure 3(*d*). The area averaged difference was reduced to about 4 K or 200 DNs when calculated from Figure 2(*a*). These increments of temperature in time are comparable to other author's finding (Ho et al. 2012). Slight differences may be due to the employed variables in our average. For the average, we used the minimum and maximum temperatures from the both satellites in contrast with the separate usage of daytime and nighttime LSTs in general.

Acknowledgments: The author thanks the Fondazione Edmund Mach for their free distribution of the programs to be used for downloading and pre-processing the LST data sets. This research was possible by the Korea Meteorological Administration Research and Development Program under the Grant KMIPA2015-5090 and by the second stage of the Brain Korea 21 Project.

References

Bonan, G. B., 2001, Observational evidence for reduction of daily maximum temperature by croplands

in the Midwest United States, *Journal of Climate*, **14**, 2430-2442, doi:http://dx.doi.org/10.1175/1520-0442(2001)014<2430:OEFROD>2.0.CO;2.

Bosilovich, M. G., 2006, A comparison of MODIS land surface temperature with in situ observations. *Geophysical Research Letters*, **33**, L20112, doi:10.1029/2006GL027519.

Cho, M.-H., K.-O. Boo, J. Lee, C. Cho, and G.-H. Lim, 2014, Regional climate response to land surface changes after harvest in the North China Plain under present and possible future climate conditions. *Journal of Geophysical Research: Atmospheres*, **119**, 4507–4520, doi:10.1002/2013JD020111.

Cooley, H. S., W. J. Riley, M. S. Tom, and Y. He, 2005, Impact of agricultural practice on regional climate in a coupled land surface mesoscale model, *Journal of Geophysics Research*, **110**, D03113, doi:10.1029/2004/jd005160.

Ge, J., 2010, MODIS observed impacts of intensive agriculture on surface temperature in the southern Great Plains. *International Journal of Climatology*, **30**, 1994-2003, doi:10.1002/joc.2093.

GRASS Development Team, 2016, Geographic Resources Analysis Support System (GRASS), GNU General Public License. http://grass.osgeo.org.

Ho, C.-H., S.-J. Park, S.-J. Jeong, J. Kim, and J.-G. Jhun, 2012, Observational evidence of double cropping impacts on the climate in the northern China plains, *Journal of Climate*, **25**, 4721-4728, doi:10.1175/JCLI-D-11-00224.1.

Jung, H.-S., G.-H. Lim, and J.-H. Oh, 2001, Interpretation of the Transient Variations in the Time Series of Precipitation Amounts in Seoul, Korea. Part I: Diurnal Variation. *Journal of Climate*, **14**, 2989-3004.

Lee, E., T. N. Chase, B. Rajagopalan, R. G. Barry, T. W. Biggs, and P. J. Lawrence, 2009, Effects of irrigation and vegetation activity on early Indian summer and monsoon variability, *International Journal of Climatology*, **29**, 573-581, doi:10.1002/joc.1721.

Lim, G.-H., and H. S. Jung, 1992: Interannual variation of the annual precipitations at Seoul, 1771–1990. *Journal of Korean Meteorological Society*, **28**, 125–132.

Menenti, M., Azzali, S., Verhoef, W., and van Swol, R., 1993, Mapping agro-ecological zones and time lag in vegetation growth by means of Fourier analysis of time series of NDVI images. *Advances in Space Research*, **5**, 233–237.

Metz, M., D. Rocchini, and M. Neteler, 2014, Surface temperatures at the continental scale: Tracking changes with remote sensing at unprecedented detail. *Remote Sensing*. **6**, 3822-3840; doi:10.3390/rs6053822, ISSN 2072-4292 www.mdpi.com/journal/remotesensing.

Nair, U. S., D. K. Ray, J. Wang, S. A. Christopher, T. J. Lyons, R. M. Welch, and R. A. Pielke Sr., 2007, Observational estimates of radiative forcing due to land use change in southwest Australia. *Journal of Geophysical Research*, **112**, D09117, doi:10.1029/2006JD007505.

Neteler M., 2010, Estimating daily land surface temperatures in mountainous environments by reconstructed MODIS LST data. *Remote Sensing*, **2**, 333-351; doi:10.3390/rs1020333. ISSN 2072-4292 www.mdpi.com/journal/remotesensing.

Osborne, T., J. Slingo, D. Lawrence, and T. Wheeler, 2009, Examining the interaction of growing crops with local climate using a coupled crop–climate model. *Journal of Climate*, 22, 1393-1411, DOI: http://dx.doi.org/10.1175/2008JCLI2494.1

Pielke, R. A. Sr., J. Adegoke, A. Beltran-Przekurat, C. A. Hiemstra, J. Lin, U. S. Nair, D. Niyogi, and T. E. Nobis, 2007, An overview of regional land use and land cover impacts on rainfall. *Tellus* B, 59, 587-601, doi:10.1111/j.1600-0889-2007.00251.x.

Ray, D. K., U. S. Nair, R. O. Lawton, R. M. Welch, and R. A. Pielke Sr., 2006, Impact of land use on Costa Rican tropical montane cloud forests: Sensitivity of orographic cloud formation to deforestation in the plains. *Journal of Geophysical Research*, **111**, D02108, doi:10.1029/2005JD006096.

Roerink, G. J., M. Menenti, and W. Verhoef, 2000, Reconstructing cloudfree NDVI composites using Fourier analysis of time series. *International Journal of Remote Sensing*, **21** (9), 1911-1917. DOI: 10.1080/014311600209814

Takata, K., K. Saito, and T. Yasunari, 2009, Changes in the Asian monsoon climate curing 1700-1850

induced by preindustrial cultivation. Proceedings of National Academy Sciences, USA, **106**(24), 9586-9589, doi:10.107/pnas.0807346106.

Yamashima, R., K. Takata, J. Matsumoto, and T. Yasunari, 2011, Numerical study of the impacts of landuse/cover changes between 1700 and 1850 on the seasonal hydroclimate in monsoon Asia. *Journal Meteorological Society of Japan*, **89A**, 291-298, doi:10.2151/jmsj.2011-A19.

Verhoef, W., M. Menenti, and S. Azzali, 1996, A colour composite of NOAA-AVHRR-NDVI based on time series (1981–1992). *International Journal of Remote Sensing*, **17**, 231–235.

Wan, Z., Y. Zhang, Q. Zhang, and Z.-L. Li, 2004, Quality assessment and validation of the MODIS global land surface temperature. *International Journal of remote sensing*, **25**, No. 1, 261-274.

Wan, Z., and Z.-L. Li, 2008, Radiance-based validation of the V5 MODIS land-surface temperature product. Source: International Journal of Remote Sensing. **29**:17, 5373-5395.

Wan, Z., Y. Zhang, Q. Zhang, and Z.-L. Li, 2004, Quality assessment and validation of the MODIS global land surface temperature. *International Journal of Remote Sensing*, **25**, No. 1, 261-274.

Zorer, R., D. Rocchini, M. Metz, L. Delucchi, F. Zottele, F. Meggio, and M. Neteler, 2013, Daily MODIS land surface temperature data for the analysis of the heat requirements of grapevine varieties. *IEEE Transactions on Geoscience and Remote Sensing*, **51**, NO. 4, 2128-2135.

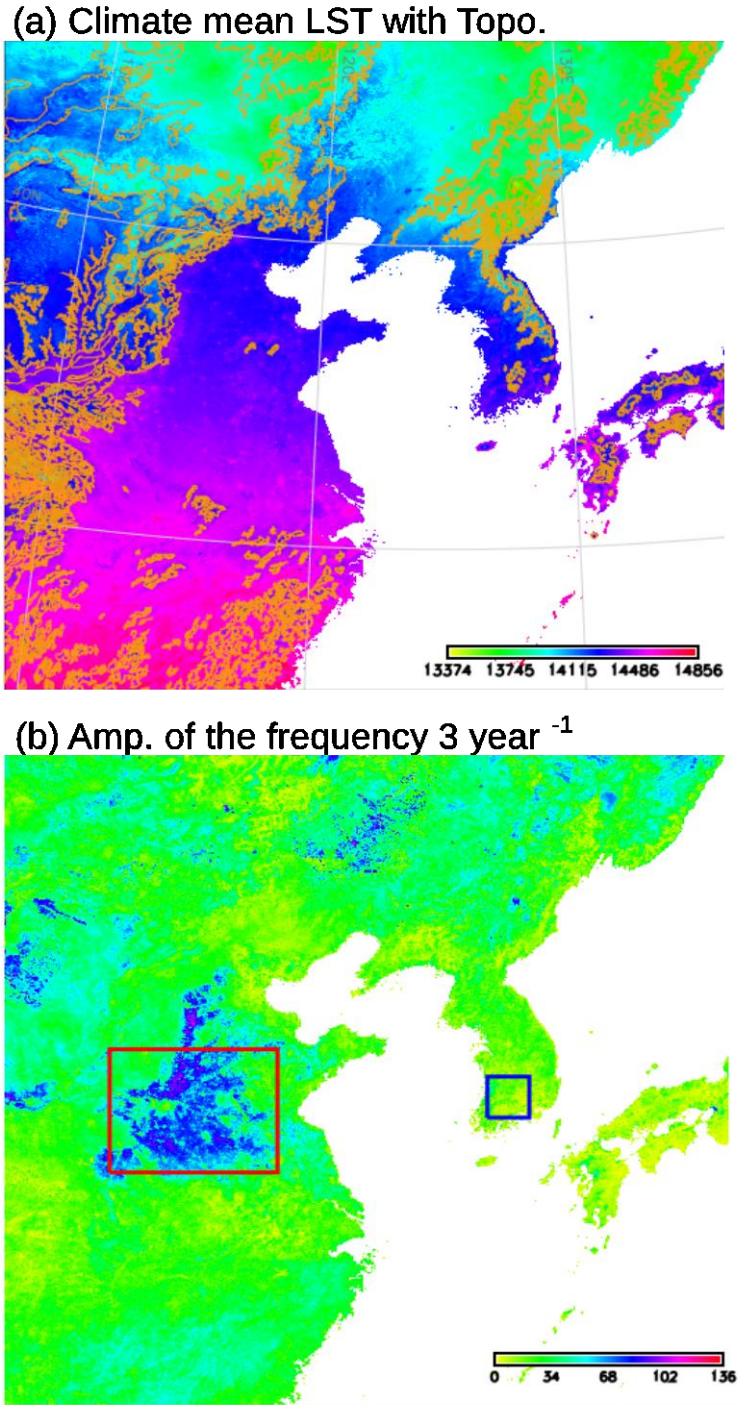

Figure 1. (*a*) Climatic mean LST in digital numbers based on Tera and Aqua 8-day minimum and maximum composites for the 11 years from 2003-2013. Topographic contours are in orange color. The contour interval is 500 meters from the zero value contours coinciding with the coastline. (*b*) Amplitudes of the frequency component 3 year^{-1} of the annual progress of LST at each pixel. In the both Figures, the pixel size is 520 m x 520 m interpolated from the LST with 1 km x 1km resolution. The red and blue rectangles mark the regions for investigating the temporal change of the 8-day LST for a year. The scale factors for colour code are in the lower right of each map.

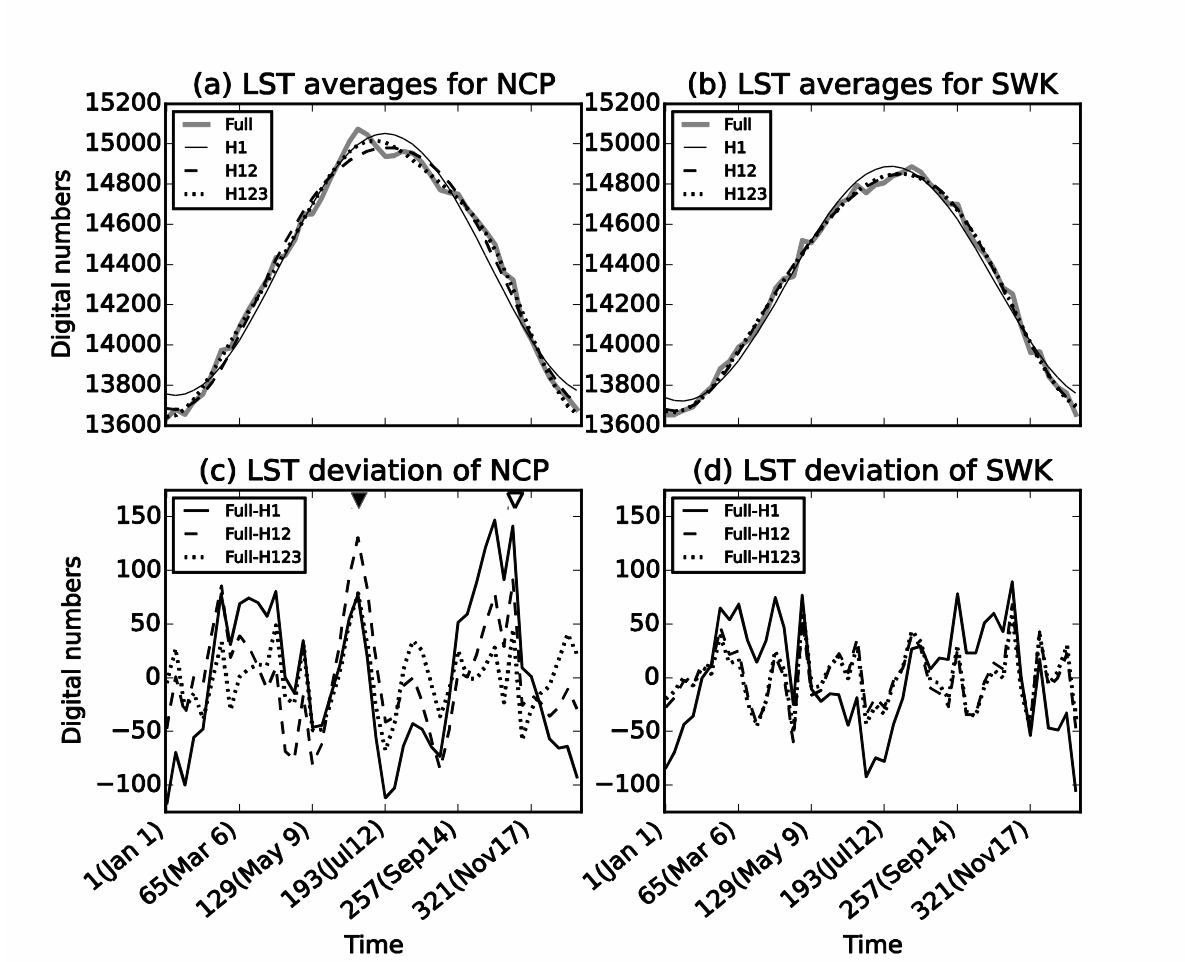

Figure 2. Area-averaged LST for the NCP (*a* and *c*) and the SWK (*b* and *d*). Figures (*a*) and (*b*) are for the LST values as a function of time predicted by various frequency components. The legend label "Full" is for the LST comprising all the frequencies (the row time series), "H1" for the frequency component 1 year^{-1}, "H12" for the components 1 year^{-1} and 2 year^{-1}, H123 for the components 1 year^{-1}, 2 year^{-1}, and 3 year^{-1}. The legend sub-label "Full-H1" means the residual or deviation of the observed LST composed with full frequencies on the value predicted by the frequency component 1 year^{-1}. Therefore, the curve with a legend "Full-H1" has all the frequencies except for the frequency 1 year^{-1}. The meaning of "Full-H12" and "Full-H123" is similar as in the previous descriptions. The solid and the empty reversed triangles denote the start time of the 8-day time interval at which the various harmonic components of spatial maps are made and displayed in Figures 3 and 4. The higher harmonics retain the frequency component 4 year^{-1} up to the Nyquist frequency. The Nyquist frequency is near 23 year^{-1} or 16-day periodicity in the analysis.

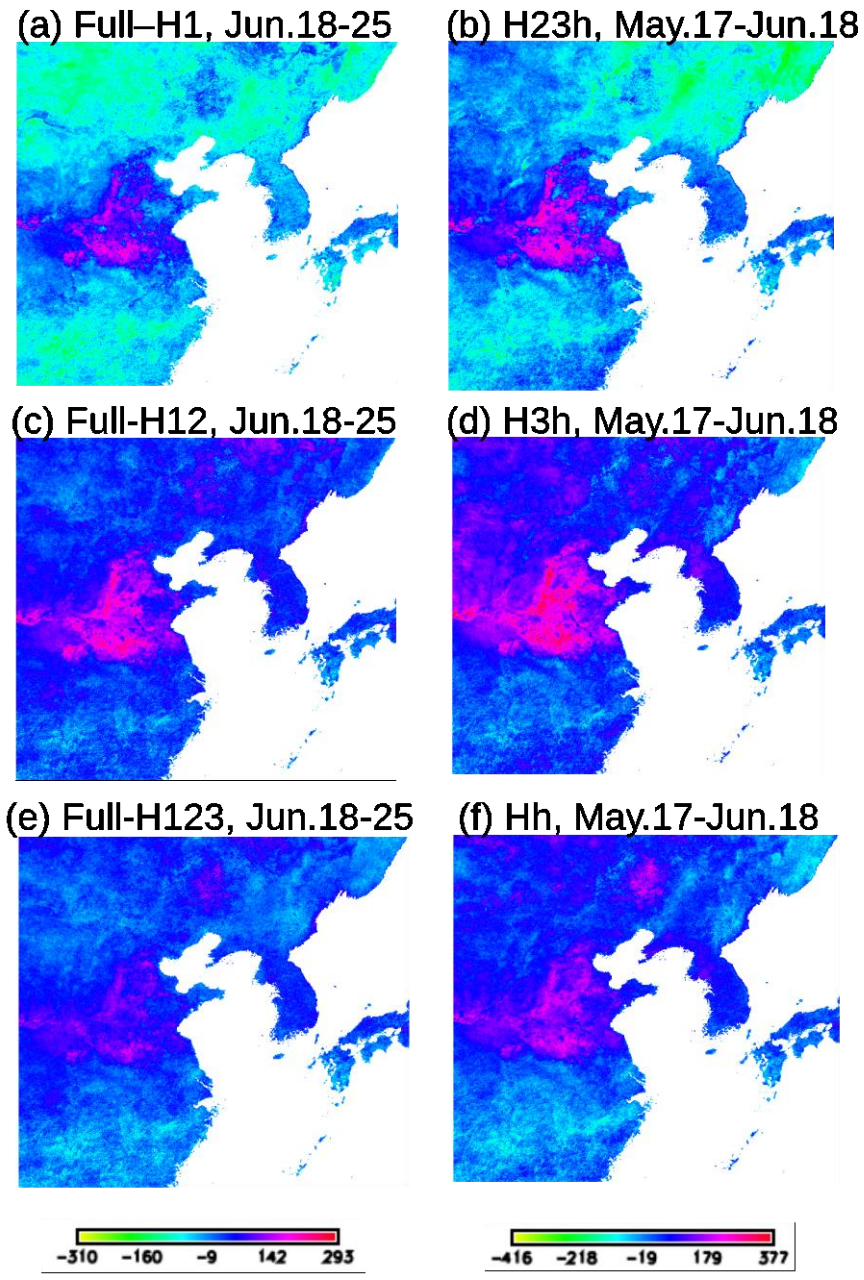

Figure 3. Distribution of the LST residuals on the calculated values based on the combination of frequencies. (*a*) The residuals from the frequency component 1 year^{-1}, (*c*) from the combination of the frequencies 1 year^{-1} and 2 year^{-1}, (*e*) from the combination of frequencies 1 year^{-1}, 2 year^{-1}, and 3 year^{-1}. The reference LST for calculation is the LST values for the time of year: DOY 169-176 or June 18-25. (*b*) Temperature increment from May 16-23 to June 17-25 for the combined contribution from the frequencies 2 year^{-1}, 3 year^{-1} and higher components, (*d*) for the frequency 3 year^{-1} and the higher frequencies, and (*f*) for the higher frequencies. The legend is in the bottom of the figure columns for the left-hand and right-hand sides, separately.